Journal of Magnetism and Magnetic Materials 330 (2013) 37–48

Contents lists available at SciVerse ScienceDirect

Journal of Magnetism and Magnetic Materials

journal homepage: www.elsevier.com/locate/jmmm

Measurement and modeling of magnetic hysteresis under field and stress application in iron–gallium alloys

Phillip G. Evans, Marcelo J. Dapino*

Department of Mechanical & Aerospace Engineering, The Ohio State University, Columbus, OH 43210, USA

ARTICLE INFO

Article history:
Received 1 March 2012
Received in revised form
22 September 2012
Available online 12 October 2012

Keywords:
Galfenol
Hysteresis
Thermodynamic model
Nonlinear characterization

ABSTRACT

Measurements are performed to characterize the hysteresis in magnetomechanical coupling of iron–gallium (Galfenol) alloys. Magnetization and strain of production and research grade Galfenol are measured under applied stress at constant field, applied field at constant stress, and alternately applied field and stress. A high degree of reversibility in the magnetomechanical coupling is demonstrated by comparing a series of applied field at constant stress measurements with a single applied stress at constant field measurement. Accommodation is not evident and magnetic hysteresis for applied field and stress is shown to be coupled. A thermodynamic model is formulated for 3-D magnetization and strain. It employs a stress, field, and direction dependent hysteron that has an instantaneous loss mechanism, similar to Coulomb-friction or Preisach-type models. Stochastic homogenization is utilized to account for the smoothing effect that material inhomogeneities have on bulk processes.

1. Introduction

Iron–gallium alloys (Galfenol) with 12–29at % gallium are an emerging class of magnetostrictive materials which have both high magnetostriction (~ 400 ppm) and ductility similar to steel [1]. This unique combination of mechanical robustness and high coupling makes Galfenol ideal for creating sensors and actuators operable in tension, bending and torsion in harsh environments. Furthermore, Galfenol can be machined, welded, extruded, and deposited into innovative geometries.

Previous studies of Galfenol magnetomechanical behavior include linear characterization [2,3] as well as a study of the nonlinear anhysteretic response [4] and reversibility [5]; a nonlinear description including hysteresis has not been published. In this work, magnetization and strain measurements of production and research grade Galfenol from Etrema Products, Inc. are presented. Measurements include applied magnetic field at constant stress, applied stress at constant magnetic field, and alternately applied magnetic field and stress. Attention is given to kinematic reversibility, referring to dependence on stress and magnetic field application order, and to thermodynamic irreversibility or the energy loss associated with magnetic hysteresis under both applied stress and magnetic field.

A previous study of reversibility by Yoo et al. [5] presents measurements with magnetic flux density and stress as independent quantities and calculates the resulting energy transduction with magnetic flux density and strain as the independent quantities. Unaccounted-for energy was attributed to "anomalous" transduction, possibly associated with the choice of independent variables. Here the independent quantities are stress and magnetic field.

The measurements presented here show a remarkable degree of kinematic reversibility in the magnetomechanical coupling, even in the production grade sample. This is in contrast with the magnetomechanical coupling in steel which has been shown to exhibit stress and field-induced magnetization that is both thermodynamically and kinematically irreversible [6,7]. The kinematic reversibility in Galfenol is demonstrated by comparing a single stress-induced magnetization curve at constant magnetic field with a series of field-induced magnetization curves at constant stress. Minor loop measurements consisting of decreasing the field from a bias point, decreasing stress from a bias point, returning the field, and returning the stress do not exhibit any observable accommodation. These measurements indicate that magnetic hysteresis for both applied field at constant stress and applied stress at constant field results from the same physical mechanism.

A new modeling framework is needed for magnetostrictive materials like Galfenol which respond in a nonlinear, anisotropic, and hysteretic manner to applied field and stress yet are kinematically reversible. While many models have been developed for ferromagnetic hysteresis and magnetomechanical coupling, a vector hysteresis model for anisotropic, magnetostrictive materials applicable for both field and stress loading is not available.

* Corresponding author. Tel.: +1 614 688 3689; fax: +1 614 292 3163.
E-mail address: dapino.1@osu.edu (M.J. Dapino).

0304-8853/$ - see front matter © 2012 Elsevier B.V. All rights reserved.
http://dx.doi.org/10.1016/j.jmmm.2012.10.002

Common approaches for modeling hysteretic materials include differential equation-based approaches derived from energy principles as in the Jiles–Atherton model [8,9] and empirical approaches like the Preisach model [10]. Scalar in its classical form, the Jiles–Atherton model has been generalized as a vector, anisotropic magnetization model as well as a scalar magnetomechanical model [11,12]. The magnetomechanical model applies to kinematically irreversible behavior which has been reported for nickel, steel, and silicon iron [6,7]. The Preisach model is also scalar in its classical form and has likewise been generalized for isotropic vector magnetization [13–15], anisotropic vector magnetization [16] and scalar stress-induced magnetization [17,18]. The Preisach model has also been used to calculate magnetostriction [19,20]. Recent work has combined aspects of the differential equations approach and the Preisach approach resulting in a model that benefits from the simplicity of the former and the generality of the latter [21]. An alternative to these classical approaches is an energy weighting approach for giant magnetostrictive materials comprising an anhysteretic vector model for both field and stress application with a scalar hysteresis mechanism [22–25]. The hysteresis mechanism uses concepts from the Jiles–Atherton model and hence inherits minor loop properties which do not agree with measurements.

Preisach-like models based on energy principles have been developed by replacing the simple Preisach hysteron which takes values of ± 1 with multi-state relays with states calculated from energy principles. In a class of vector models the states represent Stoner–Wohlfarth particle orientations which have anisotropic dependence on magnetic field [26,27]. A homogenized energy framework applicable to ferroic materials utilizes a hysteron derived from the balance of exchange and thermal energies of magnetic moments and incorporates scalar magnetic hysteresis for both field and stress application [28,29]. This framework has been extended in an anisotropic 2-D vector implementation for electrostrictive materials [30]. In general, energy-based models which utilize a Preisach-like switching mechanism provide physical insight and exhibit hysteresis properties which agree with measurements.

In this work, a formal thermodynamic development is undertaken to construct a hysteron which is applicable to magnetostrictive materials of arbitrary anisotropy. The hysteron depends on the 3-D magnetic field and stress and includes a small number of parameters, each with a clear physical interpretation. The number of hysteron states is dictated by material symmetry and anisotropy with one state for each magnetically easy axis. The criterion for switching follows from the second-law of thermodynamics and results in a unified hysteresis model which has the same properties as observed in the measurements. Following the approach of Smith et al. [28,29], a statistically distributed interaction field is superimposed on the applied field. Rather than employ a 3-D, statistically distributed coercive field, a scalar coercive energy is used in the homogenization scheme resulting in a reduction of the integration order from six to four as compared to 3-D Preisach models. This model enables accurate description of the measurements and provides a framework for understanding hysteresis in ferromagnetic materials which exhibit kinematically reversible magnetomechanical coupling.

2. Measurements

Measurements include magnetization and strain of $\langle 100 \rangle$ oriented, production and research grade Galfenol samples from Etrema Products, Inc. in cylindrical rod form with dimensions of 0.25×1 inches. In the measurement system, compressive stress is applied with an MTS 858 tabletop system by loading the sample between parallel plates. Magnetic field is applied with a drive coil situated with the Galfenol sample in a steel canister providing a flux return path. Since the permeability of Galfenol is similar to that of the steel return path, it is necessary to use a feedback controller for the magnetic field [31,32]. The changing permeability of Galfenol results in a nonlinear relationship between the voltage applied to the drive coil and the magnetic field in the Galfenol sample. Drive coil voltage is supplied by a Test Star II MTS controller. The level of voltage required to achieve a desired reference field is found by measuring the field with a Lakeshore 421 gauss meter and implementing a PI controller with an NI SCB-69 DAQ acquisition board. Magnetic flux density is measured with a Walker Scientific MF-30 fluxmeter and pick-up coil. Magnetization is calculated by subtracting the magnetic field measurement from the flux density measurement. An illustration of the measurement setup is shown in Fig. 1.

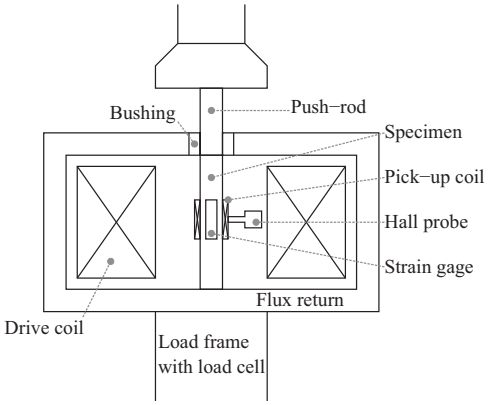

Fig. 1. Experimental setup for measuring magnetization and strain of Galfenol under magnetic field and stress.

2.1. Production Grade 18.4 at% Ga

Major magnetization loops for applied magnetic field at constant stress and applied stress at constant field are shown in Fig. 2. Magnetization versus field measurements have two regions of noticeable hysteresis, one at low fields and another at higher fields. Consider for example the curve obtained under 79 MPa compressive stress. There is a hysteretic region below 1 kA/m and another between 7 and 12 kA/m. The higher field region moves higher with increasing stress. The magnetization versus stress, at low stresses, depends strongly on the field history. The curves in Fig. 3(a) are measured after applying a positive saturating field and subsequently lowering the field to the bias point while the curves in Fig. 3(b) are measured after applying a negative saturating field and subsequently bringing the field to the bias point. In the latter, multiple loops overlap while in the former, the first loop does not close. An exception is the case where there is zero bias field after having negatively saturated the material. In this case, the negative remanence resulting from bringing the field from negative saturation to zero is wiped out by a single cycle of stress. Further cycles of the stress do not result in any magnetization change. Reported measurements of steel have a very different response, exhibiting significant accommodation with each stress cycle and a gradual convergence to a limiting loop.

Measurements shown in Fig. 4 show a remarkable degree of reversibility in the magnetomechanical coupling of Galfenol. In 4(a) a magnetization versus stress curve at constant field is obtained from direct measurement and compared to magnetization versus stress points obtained from multiple sets of magnetization versus field measurements at different bias stresses. The

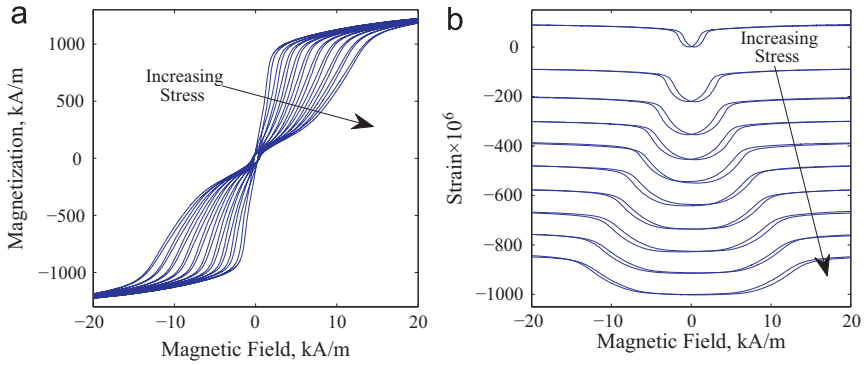

Fig. 2. (a) Magnetization and (b) strain measurements of production grade $Fe_{81.6}Ga_{18.4}$ at constant compressive stress (0, 11, 19, 26, 35, 44, 52, 61, 70 and 79 MPa).

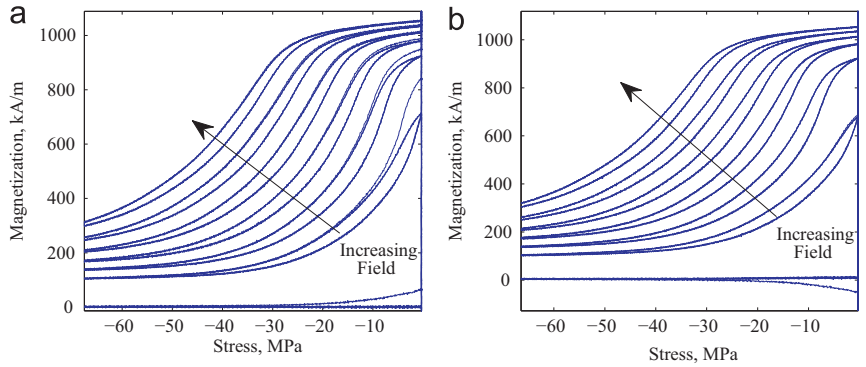

Fig. 3. Magnetization measurements of production grade $Fe_{81.6}Ga_{18.4}$ at constant field (0, 1.6, 2.4, 3.3, 4.0, 4.8, and 5.6 kA/m). (a) Bias field reached from positive saturation; (b) bias field reached from negative saturation.

points are obtained from the upper and lower branches of the magnetization versus field hysteresis curves at the given bias field. These points are then plotted versus the respective bias stresses at which the magnetization versus field curves are measured. The overlap of the curve measured directly while applying stress and the points obtained from magnetization versus field curves at constant stress suggests that the magneto-mechanical coupling is reversible and that magnetic hysteresis from applied field and applied stress results from the same physical mechanism. It also suggests that the anomalous energy found in [5] does not arise from Galfenol. Accordingly, the thermodynamic framework developed in Section 3 includes only energy transduction between the magnetic and mechanical states along with energy losses arising from domain reconfiguration.

Fig. 4(b) shows measurements from alternately applied field and stress along with two magnetization versus stress curves at constant field which are biased by first positively saturating the material and then lowering the field to the bias point. A stress is then cycled three times to a 70 MPa compression. As before, the first loop is not closed. The curve from alternate stress and field application is initialized in the same manner by saturating positive and lowering the field to 2.8 kA/m. Thus, as stress is applied it follows the magnetization versus stress curve with the higher bias field. At 12.6 MPa compression the stress is held constant and the field is lowered to 2 kA/m from its previous value of 2.8 kA/m. This moves the magnetization from the upper branch of the magnetization versus stress curve at the higher bias field to the upper branch of the magnetization versus stress curve at the lower bias. Here the field is again held constant and the stress is relaxed to 9.4 MPa resulting in a shift of the magnetization towards the lower branch of the major magnetization versus stress loop. The stress is again held constant and the field is returned to 2.8 kA/m bringing the magnetization to the lower branch of the magnetization versus stress curve obtained with a 2.8 kA/m bias field. The stress is then returned to 12.6 MPa at constant field, moving the magnetization towards the upper branch of the magnetization versus stress major loop. This stress and field cycle is repeated three times before returning the stress to zero. These minor loops obtained by alternately applying field and stress about a bias point lack any noticeable accommodation. To emphasize, this is in contrast with measurements of steel which exhibit large changes in the shape of magnetization loops obtained from cycling the stress and field [6,7].

2.2. Research grade 18.5 at% Ga

Figs. 5–7 show measurements for the research grade material. Major magnetization loops of this material have similarities with the production grade material. Specifically, the field location of the burst region is moved to higher fields with increasing bias stress (see Fig. 5(a).) The loops, however, do not have a noticeable hysteretic region at low fields as do the production grade magnetization loops. Additionally, the differential susceptibility is higher in the hysteretic burst regions. The magnetization versus stress loops (see Fig. 6(a)) are similar to the production grade measurements where the first cycle is not closed and subsequent cycles overlap. They differ in the high slope regions, having much sharper transitions. The magnetomechanical coupling in the research grade material is shown to be reversible by comparing the magnetization versus stress measured at constant field and the magnetization versus field measured at constant stress in the same manner as was done with the production grade material (see Fig. 7(a).)

The coupled nature of the hysteresis mechanism observed in the magnetization from both applied field and applied stress is emphasized in Fig. 7(b). Starting from a field of 4.2 kA/m and a compressive stress of 15 MPa, if the magnetization starts at point A on the upper branch of the major magnetization versus field

loop, increasing the stress and returning to 15 MPa pushes the magnetization to point B on the lower branch of the major loop in a single cycle. Further cycles always return to point B on the lower branch and overlap. Starting at point B on the lower branch of the hysteresis loop, when the stress is lowered to zero and brought back to 15 MPa, the magnetization is pushed to point A on the upper branch of the major loop. Further cycles always return to the upper branch of the major loop and overlap. These results show that the width of the hysteresis loops for applied stress and applied field are constrained in that knowledge of one determines the other.

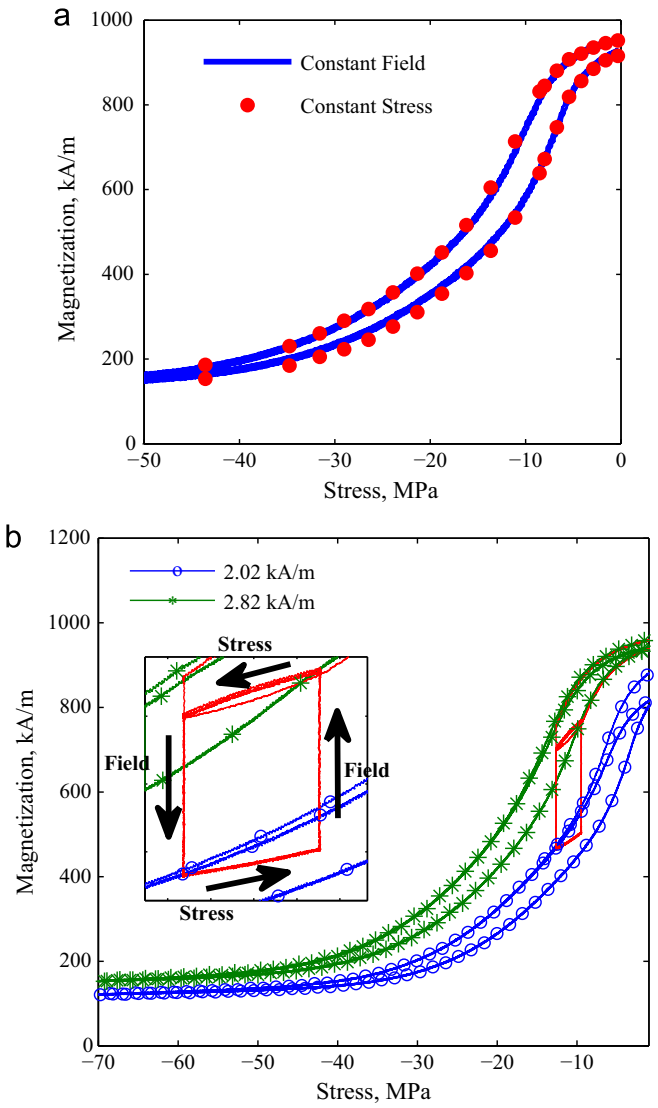

Fig. 4. (a) Comparison of production grade Fe–Ga magnetization versus stress at 2.8 kA/m field obtained from sensing and actuation measurements and (b) minor loops from alternately varying the field between 2 and 2.8 kA/m and the stress between 9.4 and 12.6 MPa compression, with the cycle repeated three times.

3. Model development

A constitutive model relating magnetization and strain to magnetic field and stress is developed from thermodynamic principles with stochastic homogenization. A hysteron for single crystalline material devoid of imperfections is first derived from thermodynamic principles. Stochastic homogenization is then employed to incorporate the smoothing effect of material inhomogeneities.

The first law of thermodynamics states that the rate of change of the internal energy U is equal to the rate of change of the applied work plus generated heat, less the heat leaving the system. For a thermomagnetomechanical material with stress $\mathbf{T}$ and strain $\mathbf{S}$ (using vector notation), magnetic field $\mathbf{H}$, magnetization $\mathbf{M}$, heat generation Q and heat flux $\mathbf{q}$, this is expressed by

$$\dot{U} = \mathbf{T}\cdot\dot{\mathbf{S}} + \mu_0\mathbf{H}\cdot\dot{\mathbf{M}} + Q - \nabla\cdot\mathbf{q}. \tag{1}$$

The second law of thermodynamics states that thermal processes result in entropy η increase. At temperature θ this can be expressed through the Clausius–Duhem inequality

$$\dot{\eta} \geq \frac{Q}{\theta} - \nabla\cdot\left(\frac{\mathbf{q}}{\theta}\right). \tag{2}$$

Eliminating the heat generation by combining the first and second laws gives

$$\theta\dot{\eta} - \dot{U} + \mathbf{T}\cdot\dot{\mathbf{S}} + \mu_0\mathbf{H}\cdot\dot{\mathbf{M}} - \frac{1}{\theta}\mathbf{q}\cdot\nabla\theta \geq 0. \tag{3}$$

The dependencies are

$$U = U(\mathbf{S},\mathbf{M},\eta), \tag{4}$$

$$\mathbf{T} = \mathbf{T}(\mathbf{S},\mathbf{M},\eta), \tag{5}$$

$$\mathbf{H} = \mathbf{H}(\mathbf{S},\mathbf{M},\eta). \tag{6}$$

In practice it is easier to measure magnetization and strain as a function of field, stress, and temperature. Furthermore, the magnetization can be interpreted as being a function of internal variables representing r possible domain orientations $\mathbf{m}^k$ each of which occurs with volume fraction ξ^k. The internal variables provide a mechanism for energy dissipation leading to a unified hysteresis mechanism for both applied field and stress. The dependencies are switched through the Legendre transformation:

$$G(\mathbf{H},\mathbf{T},\theta) = U(\mathbf{M},\mathbf{S},\eta) - \eta\theta - \mathbf{S}\cdot\mathbf{T} - \mu_0\mathbf{M}\cdot\mathbf{H}. \tag{7}$$

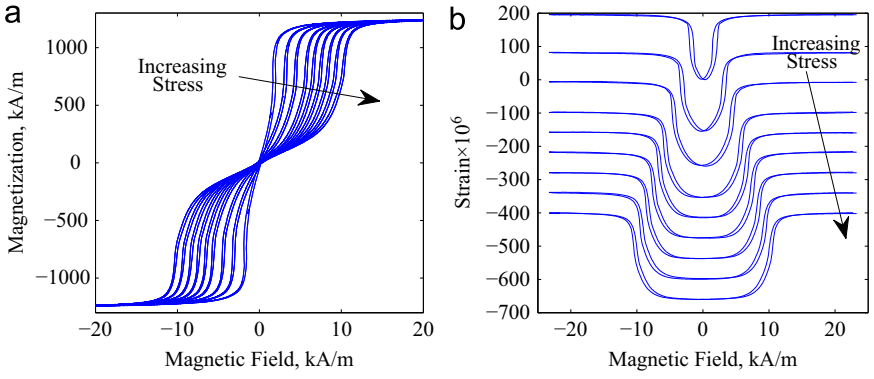

Fig. 5. Magnetization and strain measurements of research grade $Fe_{81.5}Ga_{18.5}$ at constant compressive stress (0, 9, 16, 23, 28, 32, 37, 42, and 46 MPa)

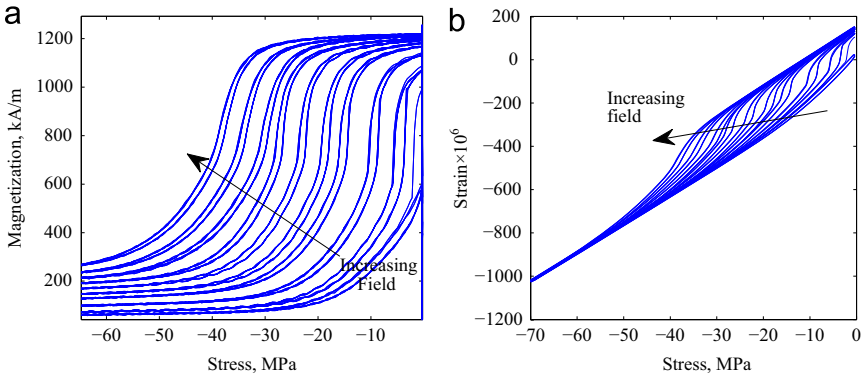

Fig. 6. Magnetization and strain measurements of research grade $Fe_{81.5}Ga_{18.5}$ at constant magnetic field (1.9, 2.4, 3.2, 4.2, 4.8, 5.6, 6.5, 7.3, 8.1, and 8.9 kA/m).

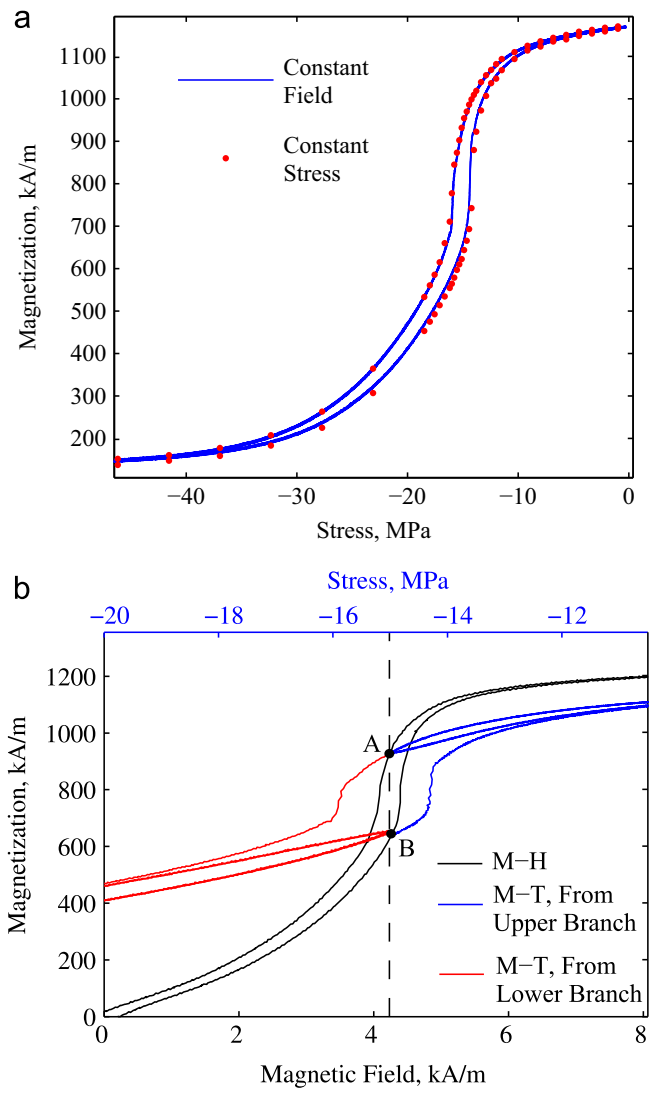

Fig. 7. (a) Comparison of research grade $Fe_{81.5}Ga_{18.5}$ magnetization versus stress at 4.2 kA/m field obtained from sensing and actuation measurements and (b) magnetization excursions from the upper and lower hysteresis branches about a bias of 15 MPa and 4.2 kA/m, cycled three times.

Since magnetization is also dependent on the internal variables $\mathbf{m}^k$ and ξ^k, the dependencies after transformation are

$$\mathbf{M}=\mathbf{M}(\mathbf{H},\mathbf{T},\theta,\mathbf{m}^k,\xi^k), \tag{8}$$

$$\mathbf{S}=\mathbf{S}(\mathbf{H},\mathbf{T},\theta,\mathbf{m}^k,\xi^k), \tag{9}$$

$$\eta=\eta(\mathbf{H},\mathbf{T},\theta,\mathbf{m}^k,\xi^k). \tag{10}$$

The time rate of change of the free energy G is then

$$\dot{G}=\frac{\partial G}{\partial \mathbf{H}}\cdot\dot{\mathbf{H}}+\frac{\partial G}{\partial \mathbf{T}}\cdot\dot{\mathbf{T}}+\frac{\partial G}{\partial \theta}\dot{\theta}+\sum_{k=1}^{r}\left[\frac{\partial G}{\partial \mathbf{m}^k}\cdot\dot{\mathbf{m}}^k+\frac{\partial G}{\partial \xi^k}\dot{\xi}^k\right]. \tag{11}$$

From (7), the time rate of change of the internal energy is

$$\dot{U}=\dot{G}+\eta\dot{\theta}+\theta\dot{\eta}+\mathbf{S}\cdot\dot{\mathbf{T}}+\mathbf{T}\cdot\dot{\mathbf{S}}+\mu_0\mathbf{H}\cdot\dot{\mathbf{M}}+\mu_0\mathbf{M}\cdot\dot{\mathbf{H}}. \tag{12}$$

Substitution of (12) and (11) into (3) gives the following restriction on thermodynamic processes resulting from changes in the independent and internal variables:

$$-\left(\eta+\frac{\partial G}{\partial\theta}\right)\dot{\theta}-\left(\mu_0\mathbf{M}+\frac{\partial G}{\partial\mathbf{H}}\right)\dot{\mathbf{H}}-\left(\mathbf{S}+\frac{\partial G}{\partial\mathbf{T}}\right)\dot{\mathbf{T}}+\sum_{k=1}^{r}\left[\frac{\partial G}{\partial\mathbf{m}^k}\cdot\dot{\mathbf{m}}^k+\frac{\partial G}{\partial\xi^k}\dot{\xi}^k\right]-\frac{1}{\theta}\mathbf{q}\cdot\nabla\theta\geq 0. \tag{13}$$

For thermomagnetomechanical materials that are thermodynamically reversible, the inequality becomes an equality and the constitutive relations can be found from

$$\mu_0\mathbf{M}=-\frac{\partial G}{\partial\mathbf{H}}, \tag{14}$$

$$\mathbf{S}=-\frac{\partial G}{\partial\mathbf{T}}, \tag{15}$$

$$\eta=-\frac{\partial G}{\partial\theta}, \tag{16}$$

$$\frac{\partial G}{\partial\xi^k}=0, \tag{17}$$

$$\frac{\partial G}{\partial\mathbf{m}^k}=0, \tag{18}$$

$$\mathbf{q}=-k\nabla\theta. \tag{19}$$

Now the following assumptions are made on the processes:

- Isothermal
- Negligible temperature gradients
- Reversible domain rotation
- Irreversible domain volume fraction evolution

With these assumptions, the following constitutive relationships are consistent with the first and second laws of thermodynamics:

$$\mu_0\mathbf{M}=-\frac{\partial G}{\partial\mathbf{H}}, \tag{20}$$

$$\mathbf{S} = -\frac{\partial G}{\partial \mathbf{T}}, \tag{21}$$

$$\frac{\partial G}{\partial \mathbf{m}^k} = 0, \tag{22}$$

$$-\frac{\partial G}{\partial \xi^k}\dot{\xi}^k \geq 0. \tag{23}$$

For this case, dissipation occurs as domains reconfigure. The free energy and volume fraction evolutions need to be defined. Given the free energy, the magnetization, strain, and possible domain orientations can be calculated from the constitutive relations (20)–(22). The volume fraction evolution must satisfy the inequality (23) in order for the thermomagnetomechanical process to satisfy the first and second laws of thermodynamics.

3.1. Energy formulation

The free energy has terms for magnetic anisotropy G_A, magnetomechanical coupling G_C, Zeeman or field energy G_Z, and elastic strain energy G_E. These energies will be expressed while idealizing the complex domain structure of ferromagnetic materials as a system of non-interacting, single-domain, Stoner–Wohlfarth (S–W) particles. Rather than employ an energy expression which is valid for all domain variants, a local definition is used for each variant which depends only on the easy axis of the variant $\mathbf{c}^k$ and its temperature dependent anisotropy coefficient $K^k(\theta)$,

$$G_A^k = \tfrac{1}{2}K^k(\theta)\left|\mathbf{m}^k - \mathbf{c}^k\right|^2. \tag{24}$$

This energy characterizes the torque required to rotate a S–W particle away from its easy axis. For small rotations, the coefficient K^k is the slope of the torque-angle curve. For cubic materials, the $\langle 100\rangle$ or $\langle 111\rangle$ directions tend to be easy. Because of crystal symmetry, the anisotropy coefficient in each direction family is the same, thus $K^k = K_{100}$ for all six $\langle 100\rangle$ directions and $K^k = K_{111}$ for all eight $\langle 111\rangle$ directions. For negative anisotropy coefficients K^k, the direction $\mathbf{c}^k$ is magnetically hard or an unstable equilibrium. For the isothermal processes considered here the anisotropy coefficients are constant.

The total anisotropy energy is the weighted sum of the contribution from each variant,

$$G_A = \sum_{k=1}^{r} G_A^k \xi^k. \tag{25}$$

The volume fraction evolution will ensure that using a locally defined anisotropy energy introduces little error into the total anisotropy energy. For magnetically soft materials, as a domain is pulled away from an easy axis, its size is reduced through domain wall motion and the size of domains lying nearer an easy axis is increased. This domain reconfiguration is modeled here through the evolution of the S–W particle volume fractions and as ξ^k decreases, the anisotropy energy contribution from the kth variant is likewise reduced.

The magnetomechanical coupling energy is the weighted sum of the contributions to the mechanical work from the magnetostriction $\boldsymbol{\lambda}^k$ of each particle variant:

$$G_C = -\sum_{k=1}^{r} (\boldsymbol{\lambda}^k \cdot \mathbf{T})\xi^k \tag{26}$$

and the Zeeman energy is the magnetic work due to each particle variant

$$G_Z = -\sum_{k=1}^{r} (\mu_0 M_s(\theta)\mathbf{m} \cdot \mathbf{H})\xi^k, \tag{27}$$

where M_s is the magnetization of a S–W particle, constant for isothermal processes. For Galfenol, the magnetostriction of a S–W particle for cubic materials is used [33]

$$\boldsymbol{\lambda}^k = \begin{bmatrix} (3/2)\lambda_{100}(\theta)(m_1^k)^2 \\ (3/2)\lambda_{100}(\theta)(m_2^k)^2 \\ (3/2)\lambda_{100}(\theta)(m_3^k)^2 \\ 3\lambda_{111}(\theta)m_1^k m_2^k \\ 3\lambda_{111}(\theta)m_2^k m_3^k \\ 3\lambda_{111}(\theta)m_3^k m_1^k \end{bmatrix}. \tag{28}$$

The spontaneous magnetostrictions in the $\langle 100\rangle$ and $\langle 111\rangle$ directions are constant for isothermal processes. The mechanical strain energy density of the material is

$$G_E = -\tfrac{1}{2}\mathbf{T} \cdot \mathbf{s}\mathbf{T}, \tag{29}$$

where the 6×6 compliance $\mathbf{s}$ has symmetry consistent with the material crystal structure. Summing the energy terms and weighting with the volume fractions, the free energy of the material is

$$G = \sum_{k=1}^{r} \xi^k G^k + \mathbf{T} \cdot \mathbf{s}\mathbf{T}, \tag{30}$$

$$G^k = \tfrac{1}{2}K^k\left|\mathbf{m}^k - \mathbf{c}^k\right|^2 - \boldsymbol{\lambda}^k \cdot \mathbf{T} - \mu_0 M_s \mathbf{m}^k \cdot \mathbf{H}. \tag{31}$$

From (20), the magnetization is

$$\mathbf{M} = -\frac{1}{\mu_0}\frac{\partial G}{\partial \mathbf{H}} = M_s \sum_{k=1}^{r} \xi^k \mathbf{m}^k \tag{32}$$

and from (21) the strain is

$$\mathbf{S} = -\frac{\partial G}{\partial \mathbf{T}} = \sum_{k=1}^{r} \xi^k \boldsymbol{\lambda}^k + \mathbf{s}\mathbf{T}, \tag{33}$$

thus to calculate the magnetization and magnetostriction, the S–W particle orientations and volume fractions need to be known.

3.2. Calculation of particle orientations

The magnetic orientations $\mathbf{m}^k$ of the S–W particles are calculated from the minimization (22). This minimization is constrained since the vector $\mathbf{m}^k$ is a unit vector. The constraint is $C = |\mathbf{m}^k| - 1 = 0$. The constrained minimization can be cast in the form of an inhomogeneous eigenvalue problem by using Lagrange multipliers, $\partial G^k/\partial \mathbf{m}^k = \gamma \partial C/\partial \mathbf{m}^k$. Gathering terms from (31) and expressing the particle free energy as $G^k = \frac{1}{2}\mathbf{m}^k \cdot \mathbf{K}^k\mathbf{m}^k - \mathbf{m}^k \cdot \mathbf{B}^k$ the eigenvalue problem is

$$(\mathbf{K}^k - \gamma\mathbf{I})\mathbf{m}^k = \mathbf{B}^k, \tag{34}$$

where the magnetic stiffness matrix $\mathbf{K}^k$ and force vector $\mathbf{B}^k$ are

$$\mathbf{K}^k = \begin{bmatrix} K^k - 3\lambda_{100}T_1 & -3\lambda_{111}T_4 & -3\lambda_{111}T_6 \\ -3\lambda_{111}T_4 & K^k - 3\lambda_{100}T_2 & -3\lambda_{111}T_5 \\ -3\lambda_{111}T_6 & \lambda_{111}T_5 & K^k - 3\lambda_{100}T_3 \end{bmatrix}, \tag{35}$$

$$\mathbf{B}^k = [c_1^k K^k + \mu_0 M_s H_1 \;\; c_2^k K^k + \mu_0 M_s H_2 \;\; c_3^k K^k + \mu_0 M_s H_2]^{\mathrm{T}}. \tag{36}$$

While the orientation can be easily solved for in terms of γ through diagonalization, determination of γ requires solution of a sixth-order polynomial obtained by substituting the γ dependent orientation into the constraint. It is important to keep the computation expense of the hysteron to a minimum since a large number of hysterons are summed in the stochastic homogenization process. To this end, the constraint is relaxed through linearization about the easy direction $\mathbf{c}^k$. This is accurate because as a field or stress pulls a particle away from the easy direction, at a critical energy level the particle flips to an equilibrium closer to the applied field or perpendicular to the applied principal

stresses. This is modeled through an instantaneous change in ξ^k. Hence particles oriented near an easy axis always have large volume fractions as compared to particles which have been rotated far from their easy axis. For the relaxed, linear constraint, the solution to the inhomogeneous eigenvalue problem is

$$\mathbf{m}^k = (\mathbf{K}^k)^{-1}\left[\mathbf{B}^k + \frac{1-\mathbf{c}^k\cdot(\mathbf{K}^k)^{-1}\mathbf{B}^k}{\mathbf{c}^k\cdot(\mathbf{K}^k)^{-1}\mathbf{c}^k}\mathbf{c}^k\right]. \tag{37}$$

The particle orientations (37) define the possible states of a 3D, anisotropic, field and stress dependent magnetization and strain hysteron. The magnetization of the hysteron is calculated from (32) and the strain from (33). An evolution equation for ξ^k will be defined in the next section. This evolution defines the switching of the hysteron states and is consistent with the second law of thermodynamics.

3.3. Evolution of domain volume fractions and hysteron development

The hysteron represents the magnetization and strain at the domain level and is constructed by tracking a single S–W particle as it switches state from an initial orientation variant $\mathbf{m}^I$ to a final orientation variant $\mathbf{m}^F$. This switching is modeled through changes in ξ^k where prior to switching $\xi^I = 1$ and $\xi^k = 0$ for $k \neq I$ and after switching $\xi^F = 1$ and $\xi^k = 0$ for $k \neq F$. Switching occurs when the energy difference $G^I - G^F := G^{IF}$ reaches a coercive energy E_c. As the field and stress change, the energy difference with the globally minimum orientation always reaches the coercive energy first, hence the state of the hysteron after switching $\mathbf{m}^F$ is always the globally minimum orientation variant. Since $\xi^k = 1$ for $k=I$ or $k=F$ and all other ξ^k are zero, from (30) the free energy of the hysteron is

$$G = \xi^I G^I + \xi^F G^F - \mathbf{s}\cdot\mathbf{T} \tag{38}$$

and the thermodynamic condition (23) which is the rate of energy dissipation becomes

$$-\frac{\partial G}{\partial \xi^I}\dot{\xi}^I - \frac{\partial G}{\partial \xi^F}\dot{\xi}^F = -G^I\dot{\xi}^I - G^F\dot{\xi}^F \geq 0. \tag{39}$$

The criterion for switching from $\mathbf{m}^I$ to $\mathbf{m}^F$ can be expressed mathematically as a dirac-delta function:

$$\dot{\xi}^F = \delta(G^{IF} - E_c), \quad \dot{\xi}^I = -\dot{\xi}^F. \tag{40}$$

The energy dissipation becomes

$$-G^I\dot{\xi}^I - G^F\dot{\xi}^F = G^I\dot{\xi}^F - G^F\dot{\xi}^F = G^{IF}\dot{\xi}^F = G^{IF}\delta(G^{IF}-E_c) = \begin{cases} E_c, & G^{IF} = E_c \\ 0, & \text{else.} \end{cases} \tag{41}$$

Thus there is an instantaneous energy dissipation of E_c when switching occurs. A hysteron for changing field or stress is constructed as follows. For each time step, the orientations $\mathbf{m}^k$ are calculated from (37) and the particle energies G^k from (31). The initial state $k=I$ must be known. The final state $k=F$ is taken as the globally minimum state. After a step change in the field or stress, the hysteron state either stays as $k=I$ or switches to $k=F$ if the switching criterion is met. The magnetization and strain of the hysteron are then calculated from (32) and (33), in other words, the magnetization before and after switching is $M_s\mathbf{m}^I$ and $M_s\mathbf{m}^F$ and the magnetostriction before and after switching $\boldsymbol{\lambda}^I$ and $\boldsymbol{\lambda}^F$ where $\boldsymbol{\lambda}^k$ is given by (28) for cubic materials.

3.4. Reduction of vector hysteron to scalar hysterons

The classical Preisach model is scalar and depends on magnetic field only. The Preisach relay switches between two field independent states, ± 1 representing domains as oriented up and down. Switching occurs at a field value of $H = \pm H_c$ where H_c is the coercive field and the magnetization contribution of the relay is $\pm M_s$. For the hysteron presented here, consider a material with uniaxial anisotropy having easy axes in the $[\pm 100]$ directions. Associated with these two easy axes are two variants of S–W particle orientations, $\mathbf{m}_{[100]}$ and $\mathbf{m}_{[\bar{1}00]}$ having the same anisotropy constant, K_{100}. If the field is applied in the direction $\mathbf{u} = [1\ 0\ 0]$, then the hysteron reduces to the classical Preisach relay. From Eq. (37), the component of the variant $\mathbf{m}_{[100]}$ is $+1$ in the direction of $\mathbf{u}$, i.e. $\mathbf{u}\cdot\mathbf{m}_{[100]} = 1$ and the component of the variant $\mathbf{m}_{[\bar{1}00]}$ is -1. No rotation of the S–W particles occurs with field application because it is applied along the easy axes. The energies of the two variants are $\mp\mu_0 M_s H - 1/2K$ giving the energy difference between the two variants as $G_{[\bar{1}00]} - G_{[100]} = 2\mu_0 M_s H$. Therefore the hysteron switches from the $[\bar{1}00]$ direction to the [100] direction at the coercive field $H_c = E_c/(2\mu_0 M_s)$.

Smith's homogenized energy model [28] employs two energy-based hysterons—one for static operation and another which has rate-dependence characterizing the thermal after-effect . The static hysteron differs from the Preisach relay in that up and down states vary linearly with field. This same relay behavior can be achieved with the proposed hysteron here by again considering uniaxial material but applying the field away from the easy axes. Examples are shown in Fig. 8 with the field applied 0°, 30°, 60°, and 90° from the easy axis in the [100] direction. At an increasing angle the hysteron reflects greater difficulty in magnetizing since the direction is further away from the easy axes. At 90° the two variants have the same orientation and energy and no switching occurs. For an angle θ the slope or relative susceptibility of the up and down states is

$$\chi = \sin^2(\theta)\frac{\mu_0 M_s}{K_{100}} \tag{42}$$

and the remanence is $\pm\cos\theta$. The energy difference is $G_{[\bar{1}00]} - G_{[100]} = 2\cos(\theta)\mu_0 M_s H$ which results in a coercive field for switching from the down to the up state $H_c = E_c/(2\cos(\theta)\mu_0 M_s)$. This anisotropic hysteron illustrates an important difference between Preisach models and homogenized energy models. Both employ an elementary hysteron with statistically distributed parameters, however, the former includes effects from additional physics such as anisotropy or magnetomechanical coupling in the density functions while the latter includes additional physics in the hysteron, which describes the underlying material behavior. Typically this results in simpler density functions, or in the discretized model, fewer weights.

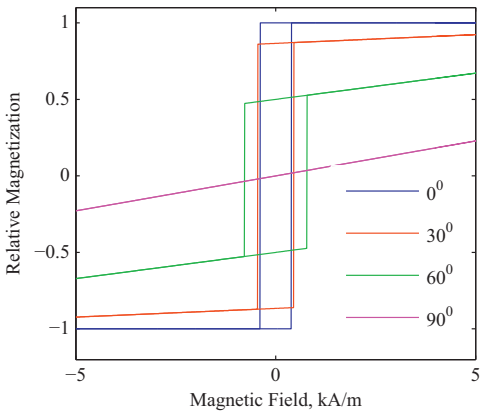

Fig. 8. Anisotropic hysterons.

3.5. Description of measurements with elementary hysteron

The hysteron can describe the underlying shape of the magnetization versus field curves in Figs. 2(a) and 5(a) as well as the magnetization versus stress curves in Figs. 6(a) and 3(a) and (b). Even though the measurements are unidirectional, a vector model is needed for their description because anisotropic, 3-D domain rotation occurs.

For ⟨100⟩ oriented, research grade material a ⟨100⟩ orientation is aligned with the rod axis which is the direction of field and stress. The stress dependence of the hysteretic burst regions in Fig. 5(a) can be understood from the hysterons in Fig. 9(a). The low-field linear region is due to rotation of ⟨100⟩ domains perpendicular to the field direction. The hysteron represents this region through the field and stress dependence given by (37) of $\mathbf{m}^k$ which have easy axes perpendicular to the field. There are four such $\mathbf{m}^k$ which explains why the hysteron has only three unique states when calculating magnetization and strain in a ⟨100⟩ direction. The burst region occurs by domain reconfiguration as the size of domains along the ⟨100⟩ direction aligned with the field grows at the expense of the perpendicular domains. In the hysteron, the burst region is described by switching from $\mathbf{m}^I$ with easy axes perpendicular to the field to $\mathbf{m}^F$ with the easy axis parallel to the field. The coercive or dissipation energy E_c causes a delay which accounts for the noticeable hysteresis in the burst region and lack thereof in the low-field region where the magnetization process is dominated by domain rotation. With increased stress, the energy of $\mathbf{m}^k$ with easy axes perpendicular to the field is decreased, thus the field location where switching occurs is pushed to higher fields.

The additional hysteretic region at low fields for the production grade, field applied major loops results from misalignment. Two of the ⟨100⟩ easy directions near the plane perpendicular to the rod axis are closer to the negative rod direction and the other two are closer to the positive rod direction. Thus hysteretic switching occurs between these orientation variants as the field crosses zero (see Fig. 10(a)). Although this switching results in energy loss, it does not result in a low-field hysteresis region for the magnetostriction (see Figs. 2 and 10) because magnetostriction is a quadratic relation; the variants which are slightly closer to the positive field direction and the variants which are slightly closer to the negative field direction have the same magnetostriction.

The center of the burst region in the magnetization versus field measurements can be calculated analytically from $G^I = G^F$ and the susceptibility in the low field, domain rotation region, can be calculated from (37). The anisotropy coefficient K_{100} can be determined directly from the measurements since (37) is an analytical function of K_{100} . The particle magnetization M_s and the magnetostriction λ_{100} can be directly found from the saturation magnetization and magnetostriction values. The shear magnetostiction coefficient λ_{111} does not affect [100] behavior because no shear stresses are present. The coercive energy can be found from the areas of the hysteretic regions which give the energy loss. The values for the hysteron parameters are in Table 1.

Magnetization versus stress loops in Figs. 6(a) and 3(a) and (b) can be understood from the hysterons in Fig. 9(b). Stress causes domain switching from the bias field direction or high state to the perpendicular plane or low state. At low stresses, when the material has been saturated positively prior to application of the bias field, if the hysteron is double-valued, it will be at the high state. Application of stress switches the hysteron to the low state and upon removal of the stress it remains in the low state. In subsequent loops, the hysteron starts and ends in the low state. This accounts for the observed non-closure of the first loop and closure of all subsequent loops; it is due to the history of the domain configuration. When the material is saturated negatively

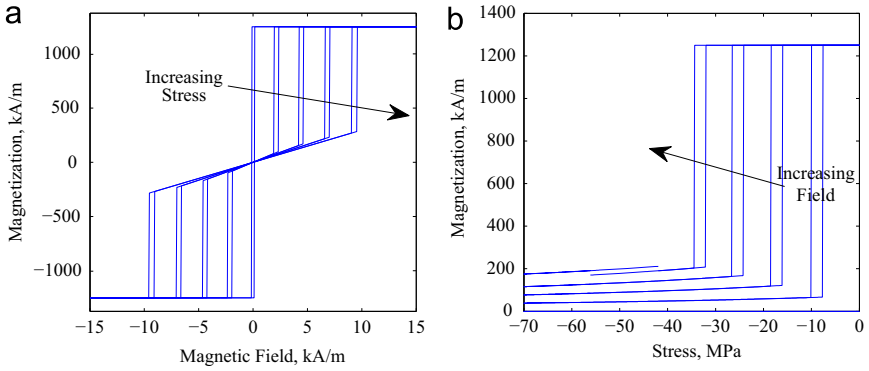

Fig. 9. Magnetization of a hysteron in the [100] direction for (a) applied field at constant stress and (b) applied stress at constant field.

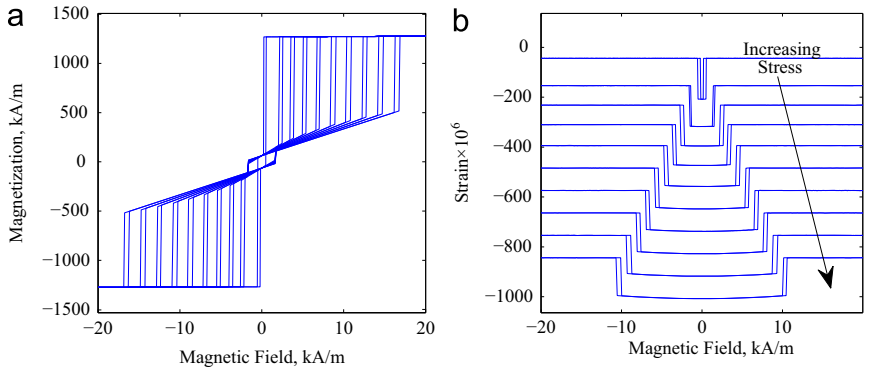

Fig. 10. Hysteron calculations of (a) magnetization and (b) strain in the near [100] direction for applied field at constant stress.

Table 1
Hysteron parameters for production grade $Fe_{81.4}Ga_{18.6}$ and research grade $Fe_{81.5}Ga_{18.5}$.

Grade	$\mu_0 M_s$ (T)	K_{100} (kJ/m^3)	E_c (J/m^3)
Research	1.55	35	218
Production	1.6	35	192
	$\lambda_{100} \times 10^6$	$\lambda_{111} \times 10^6$	E (GPa)
Research	177	N/A	76.5
Production	110	3	98

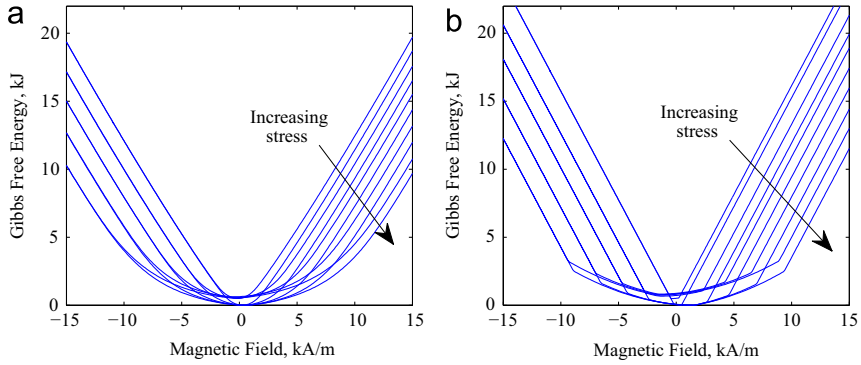

Fig. 11. Dependence of Gibbs free energy on [100] field and stress for the $Fe_{81.6}Ga_{18.4}$, production grade sample, calculated from (a) the measurements and (b) the model with a single hysteron; compressive bias stresses are 0, 19, 35, 52, and 70 MPa.

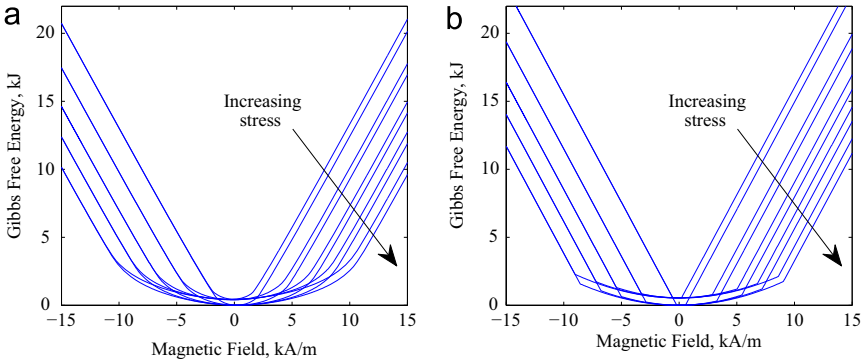

Fig. 12. Dependence of Gibbs free energy on [100] field and stress for the $Fe_{81.5}Ga_{18.5}$, research grade sample, calculated from (a) the measurements and (b) the model with a single hysteron; compressive bias stresses are 0, 16, 28, 37, and 46 MPa.

prior to bias field application, the hysteron starts in the low state and hence the first loop is closed also. A departure from this pattern occurs when the bias field is zero. In this case the hysteron begins negative, described by the $\mathbf{m}^I$ with easy axis oriented in the negative field direction. Applied stress switches the hysteron state to $\mathbf{m}^F$ with easy axis perpendicular to the bias field. Further cycles do not result in magnetization change because there is no field causing a preference for either the positive or negative rod directions. Thus the remanent magnetization of materials with kinematically reversible magnetomechanical coupling can be completely eliminated with a single stress cycle which forces all domains to the perpendicular plane. For sufficiently high bias fields, the hysteron is not double-valued at zero stress and thus there is no distinction between saturating the material positively or negatively; in both cases, the starting and ending domain configuration is all domains aligned in the bias field direction.

The dependence of the Gibbs free energy on [100] directed field can be calculated from the measurements by numerically integrating (20); the free energy calculated from applied field measurements is compared with the free energy of a hysteron in Figs. 11 and 12 for the research and production grade samples, respectively. Just as a single Preisach relay is blocky compared to magnetization-field loops, the energy calculated from a single hysteron has much sharper transitions than the measurements. The energy loss associated with hysteretic domain reconfiguration causes a difference between the beginning and ending energy level which is characterized in the hysteron through the parameter E_c. For a full major loop of the research grade material, the hysteron switches four times and for the production grade material six switches occur, i.e. two switches occur for each hysteresis region—one on the up-side and one on the down-side . The five energy versus field curves for the research grade sample (calculated at different bias stresses) have nearly the same energy loss with an average of 873 J/m^3 which gives a value of 218 J/m^3 for E_c (a fourth of the loop energy loss.) The five energy versus field curves for the production grade sample have an average energy loss of 1,149 kJ/m^3 giving a value of 192 J/m^3 for E_c (a sixth of the loop energy loss.) Though the estimation of E_c is less for the production grade sample, the total energy loss is greater since more switching occurs owing to the low field hysteresis region. Despite this, the comparison is still unexpected and may result from describing the data with a single hysteron. In the next section, stochastic homogenization is employed where

statistical variation in E_c and the magnetic field are considered. Then, a collection of hysterons is considered and the energy loss in a major loop is the average value of the product of the number of switches occurring in a hysteron and E_c.

The dependence of the Gibbs free energy on [100] directed stress can be calculated from the measurements by numerically integrating (21). A comparison between the measurements and the free energy of a single hysteron is shown in Fig. 13 at four different bias fields. Stress–strain data for the production grade sample is not available. For the research grade sample, three stress cycles were performed starting at zero stress at each bias field. Energy is lost for each cycle resulting in a downward shift of the energy of an amount $2E_c$ since two switches occur—the up and the down switches between the directions parallel to the field and near perpendicular to the field. The average loss per cycle for the four measurements is 659 J/m^3 which is less than for applied field major loops. That the loss per loop is less than for the applied field measurements is expected since fewer switches or domain reconfigurations occur. According to the model the loss per loop should be exactly half since half as many switches take place. Since it is not exactly half, this suggests the presence of a small amount of energy loss from purely mechanical hysteresis which is neglected here where the purely mechanical strain is modeled through Hooke's law or a quadratic strain energy density.

3.6. Stochastic homogenization

Material inclusions and lattice imperfections cause variations in the local magnetic field and coercive energy [28]. This variation is modeled using a statistically distributed interaction field $\mathbf{H}_I$, superimposed on the macroscopic applied field $\mathbf{H}$. The macroscopic magnetization and strain can be calculated through stochastic homogenization of the interaction field and coercive energy:

$$\overline{\mathbf{M}}(\mathbf{H},\mathbf{T}) = \int_0^\infty \int_{-\infty}^\infty \mathbf{M}(\mathbf{H}+\mathbf{H}_I,\mathbf{T},E_c)v(\mathbf{H}_I,E_c)\, d\mathbf{H}_I\, dE_c, \tag{43}$$

$$\overline{\mathbf{S}}(\mathbf{H},\mathbf{T}) = \int_0^\infty \int_{-\infty}^\infty \mathbf{S}(\mathbf{H}+\mathbf{H}_I,\mathbf{T},E_c)v(\mathbf{H}_I,E_c)\, d\mathbf{H}_I\, dE_c. \tag{44}$$

The homogenization procedure (43) is similar to the homogenized energy model of Smith et al. [28] when thermal activation is neglected. Different energy potentials are used for the hysterons and the energy formulation here is done in 3-D . Additionally, a coercive energy consistent with the second law of thermodynamics was defined rather than a coercive field. This homogenization procedure has a distinct computational advantage over the vector implementation of Preisach models. Vector Preisach models for 3-D magnetization-field behavior use six statistically distributed parameters, two for each dimension which dictate when switching occurs from up to down and visa versa. The model proposed here includes four statistically distributed parameters meaning that the model implementation requires quadruple integration rather than the sextuple integration required for vector models using the classical Preisach model.

The procedure here offers the additional advantage of simpler density functions since the effects of anisotropy and stress are incorporated in the hysteron behavior rather than the densities. Consider again the case of uniaxial anisotropy for which the hysterons are shown in Fig. 8. Since the physical information regarding anisotropy is embedded in the hysteron, a simple Gaussian distribution of each component of the interaction field can be used. Fig. 14 shows the homogenized model with a Gaussian distribution; the behavior is anisotropic even though all three components of the interaction field have the same standard deviation. An exponential distribution was used for the coercive energy.

3.7. Comparison with experiments

Here, the homogenized energy model is compared with research grade measurements. The hysteron parameters in Table 1 are used. The discretized probability density in the homogenized energy model (43) is found through least-squares optimization to a single $\mathbf{M}-\mathbf{H}$ curve, measured with a 23 MPa compressive bias stress. The procedure for identifying a general density, described in [34], is used. The integrals are performed over small segments using Gauss-quadrature . The bounds of the integrals for the interaction field are the fields required for positive and negative saturation, ± 10 kA/m. The bound for the coercive energy was chosen as 600 J/m^3, over twice

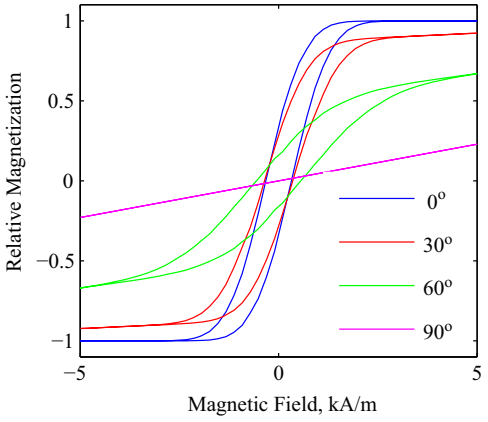

Fig. 14. Stochastic homogenization of the anisotropic, vector magnetization model.

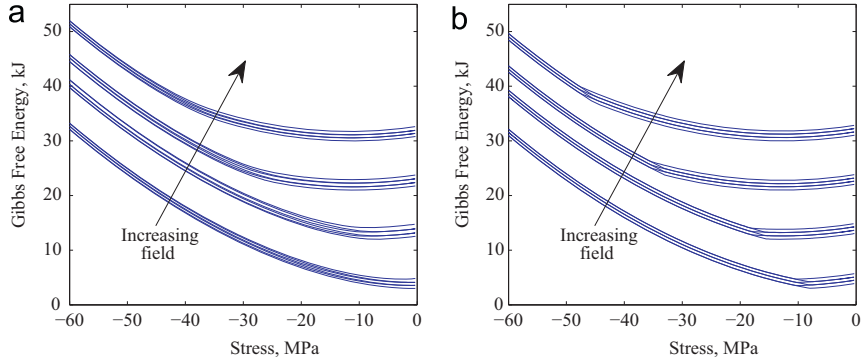

Fig. 13. Dependence of Gibbs free energy on [100] field and stress for the $Fe_{81.5}Ga_{18.5}$, research grade sample, calculated from (a) the measurements and (b) the model with a single hysteron; bias fields are 1.9, 3.2, 6.5 and 8.9 kA/m.

the value used for a single hysteron in Section 3.5. This bound was chosen so that the value of $v(\mathbf{H}_l,E_c)$ is approximately zero at the bounds. This condition is necessary to ensure that the error introduced by using finite integral bounds is minimal. The Gauss quadrature rules give the hysteron evaluation points $(H_l)_{1,i}$, $(H_l)_{2,j}$, $(H_l)_{3,k}$, $E_{c,l}$ and weights w_{ijkl}. The hysteron values are then calculated at each of the Gauss points $\mathbf{M}(\mathbf{H}+\mathbf{H}_l,\mathbf{T},E_c)_{ijkl}$. The values of the density at each Gauss point, v_{ijkl} are found through the least-squares optimization routine lsqnonlin in Matlab. The objective function for the routine is the error between the model and the measurements. The model value of magnetization for each applied field and stress value are calculated with the summation over the four indices, $\mathbf{M}(\mathbf{H}+\mathbf{H}_l,\mathbf{T},E_c)_{ijkl}(vw)_{ijkl}$, which approximates the fourth-order integration. The strain is calculated similarly, but not used in the optimization scheme.

To illustrate the accuracy and properties of the model, the density is first found from optimizing for the error between the model and the measured magnetization values for applied field at a constant compression of 23 MPa. A comparison with the model is then made between the measured strain of this same experiment along with the magnetization and strain of a separate experiment of applied stress at a constant magnetic field of 4.8 kA/m. The result is displayed in Fig. 15. The density is only optimized for the measurements in Fig. 15(a), yet there is excellent agreement between the model and the measurements in Fig. 15(b) and (c). This confirms that the hysteron describes the underlying physical behavior since from figure to figure, the density remains the same and only the hysteron changes. Though the density was found from measurements for applied field at constant stress, the model accurately describes the measurements for applied stress and constant field. Fig. 16 shows that the hysteresis properties of the model agree with the measurements. Starting from the lower branch of a magnetization-field major loop, a cyclic reduction in the stress pushes the magnetization to the upper branch in a single cycle with subsequent cycles

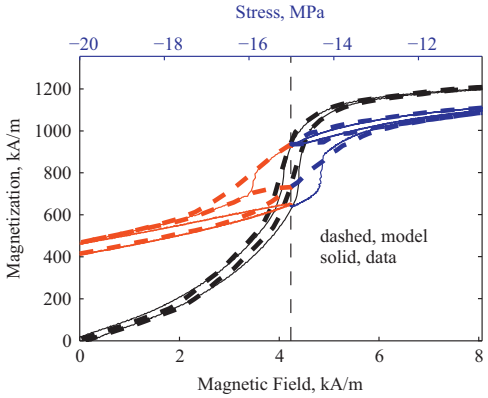

Fig. 16. Magnetization excursions from the upper and lower hysteresis branches about a compressive bias of 15 MPa and 4.2 kA/m, cycled three times.

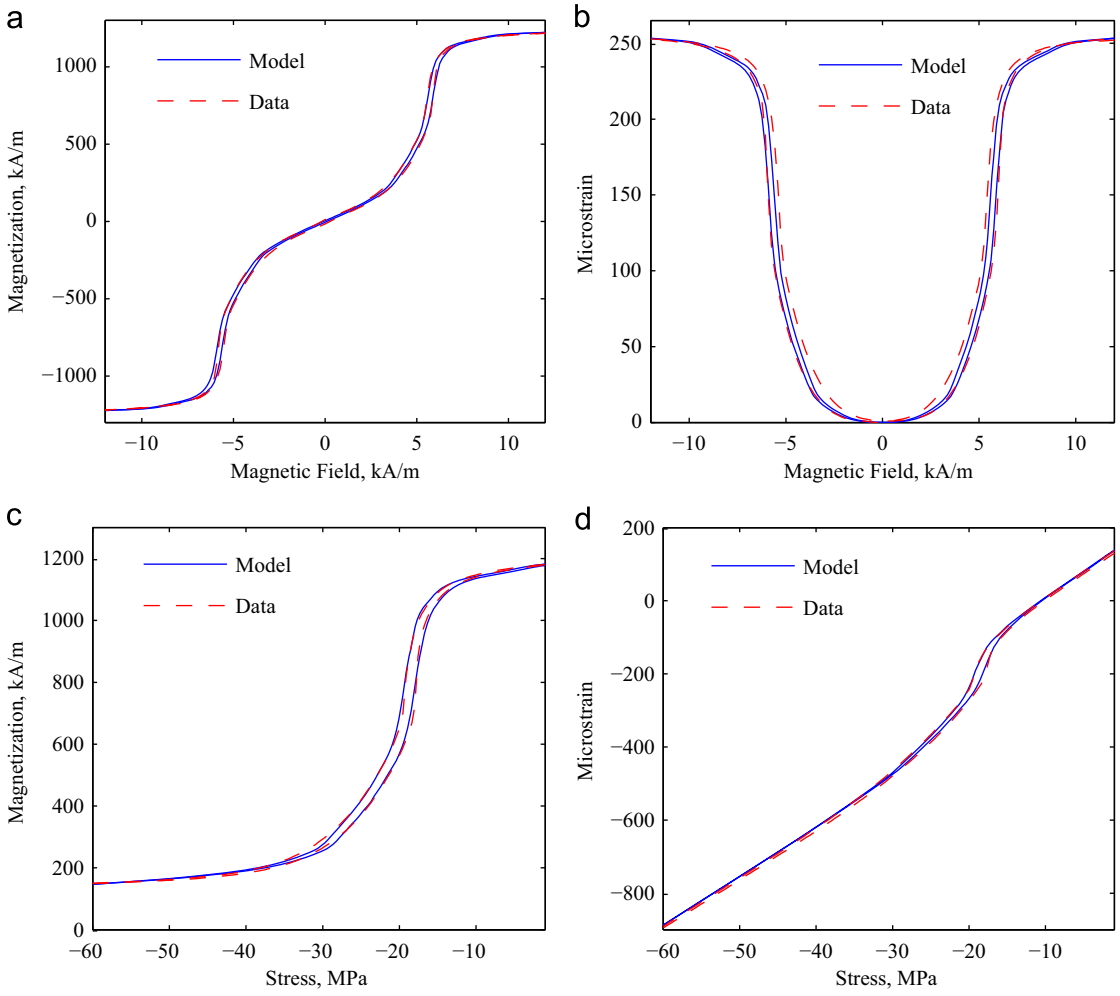

Fig. 15. Model and measured magnetization and strain from (a), (b) applied field at a compression of 23 MPa, and (c), (d) applied stress at a bias field of 4.8 kA/m.

returning to the upper branch. Starting from the upper branch, a cyclic increase in the stress pushes the magnetization to the lower branch with subsequent cycles returning to the lower branch. The coupled nature of the hysteresis as well as the nonclosure of initial loops is described by the model through the history of magnetic domain orientations.

4. Concluding remarks

Measurements were presented to characterize the coupled nonlinear and hysteretic magnetization and strain of production and research grade Galfenol due to applied stress and field. It was shown that hysteresis for both applied quantities can be attributed to the same physical mechanism and that major magnetization versus stress loops in compression depend heavily on magnetic history at low stress levels. Remarkable reversibility in the magnetomechanical coupling was demonstrated by generating the same magnetization versus stress hysteresis loop both from a series of constant stress experiments and from a single constant field experiment. Cyclic application of alternately applied field and stress did not result in any noticeable accommodation, i.e. Galfenol constitutive behavior is kinematically reversible.

A thermodynamic framework, satisfying the first and second laws of thermodynamics, was developed to describe the observed nonlinear and hysteretic behavior. Like the measurements, magnetization and strain calculations from the model are thermodynamically irreversible and kinematically reversible. Hysteresis was attributed to energy loss during the process whereby the volume fractions of differently oriented domains change. This process was modeled by tracking the orientation of a number of elementary hysterons whose states represent the energetically possible domain orientations. The hysteron is 3-D, anisotropic, and both stress and field dependent. The model thereby does not depend on complex density functions to describe these effects, as do models based on the classical Preisach model. An additional advantage over Preisach models is that hysteron switching is characterized by a coercive energy rather than a 3-D coercive field. As a result, the integration order is four rather than six. The model provides a physical and accurate description of 3-D magnetic and strain hysteresis for anisotropic magnetostrictive materials.

Acknowledgments

We wish to acknowledge the financial support by the Office of Naval Research, MURI grant #N000140610530. Measurements were performed at the Naval Surface Warfare Centery, Carderock Division as part of the Naval Research Enterprise Internship Program for P.G.E., with Marilyn Wun-Fogle and Dr. James Restorff as mentors.

References

[1] R. Kellogg, A. Russell, T. Lograsso, A. Flatau, A. Clark, M. Wun-Fogle, Tensile properties of magnetostrictive iron-gallium alloys, Acta Materialia 52 (2004) 5043–5050.
[2] R. Kellogg, A. Flatau, A. Clark, M. Wun-Fogle, T. Lograsso, Quasi-static transduction characterization of Galfenol, Journal of Intelligent Material Systems and Structures 16 (2005) 471–479.
[3] M. Wun-Fogle, J. Restorff, A. Clark, Magnetomechanical coupling in stress-annealed Fe–Ga (Galfenol) alloys, IEEE Transactions on Magnetics 42 (10) (2006) 3120–3122.
[4] J. Atulasimha, A. Flatau, E. Summers, Characterization and energy-based model of the magnetomechanical behavior of polycrystalline iron–gallium alloys, Smart Materials and Structures 16 (2007) 1265–1276.
[5] J. Yoo, G. Pelligrini, S. Datta, A. Flatau, An examination of Galfenol mechanical magnetic coupling coefficients, Smart Materials and Structures 20 (2011) 075008.
[6] K. Pitman, The influence of stress on ferromagnetic hysteresis, IEEE Transactions on Magnetics 26 (5) (1990) 1978–1980.
[7] D. Craik, M. Wood, Magnetization changes induced by stress in a constant applied field, Journal of Physics D Applied Physics 3 (1970) 1009–1016.
[8] D. Jiles, D. Atherton, Theory of ferromagnetic hysteresis, Journal of Magnetism and Magnetic Materials 61 (1–2) (1986) 48–60.
[9] D. Jiles, Introduction to Magnetism and Magnetic Materials, Chapman and Hall, London, UK, 1995.
[10] F. Preisach, Uber die magnetische nachwirkung, Zeitschrift fur Physik 94 (1935) 277–302.
[11] A. Bergqvist, A simple vector generalization of the Jiles–Atherton model of hysteresis, IEEE Transactions on Magnetics 32 (5) (1996) 4213–4215.
[12] D. Jiles, J. Thoelke, Theoretical modelling of the effects of anisotropy and stress on the magnetization and magnetostriction of $Tb_{0.3}Dy_{0.7}Fe_2$, Journal of Magnetism and Magnetic Materials 134 (1) (1994) 143–160.
[13] I. Mayergoyz, G. Friedman, Isotropic vector Preisach model of hysteresis, Journal of Applied Physics 61 (8) (1987) 4022–4024.
[14] A. Adly, I. Mayergoyz, A. Bergqvist, Preisach modeling of magnetostrictive hysteresis, Journal of Applied Physics 69 (8) (1991) 5777–5779.
[15] A. Adly, I. Mayergoyz, A new vector Preisach-type model of hysteresis, Journal of Applied Physics 73 (10) (1993) 5824–5826.
[16] E.D. Torre, F. Vajda, Vector hysteresis modeling for anisotropic recording media, IEEE Transactions on Magnetics 32 (3) (1996) 1116–1119.
[17] A. Bergqvist, G. Engdahl, A phenomenological magnetomechanical hysteresis model, Journal of Applied Physics 75 (10) (1994) 5496–5498.
[18] G. Bolshakov, A. Lapovok, A Preisach model for magnetoelastic hysteresis, Journal of Magnetism and Magnetic Materials 162 (1996) 112–116.
[19] L. Dupré, R.V. Keer, J. Melkebeek, Evaluation of magnetostrictive effects in soft magnetic materials using the Preisach theory, Journal of Magnetism and Magnetic Materials 254–255 (2003) 121–123.
[20] A. Reimers, E.D. Torre, Fast Preisach based magnetosriction model for highly magnetostrictive materials, IEEE Transactions on Magnetics 35 (3) (1999) 1239–1242.
[21] F. Ossart, O. Hubert, R. Billardon, A new internal variables scalar hysteresis model respecting the wiping-out property, Journal of Magnetism and Magnetic Materials 254–255 (2003) 170–172.
[22] W. Armstrong, Magnetization and magnetostriction processes in $Tb_{0.27-0.30}Dy_{0.73-0.70}Fe_{1.9-2.0}$, Journal of Applied Physics 81 (5) (1997) 2326–23217.
[23] W.D. Armstrong, An incremental theory of magneto-elastic hysteresis in pseudo-cubic ferro-magnetostrictive alloys, Journal of Magnetism and Magnetic Materials 263 (2003) 208.
[24] J. Atulasimha, G. Akhras, A. Flatau, Comprehensive 3-D hysteretic magneto-mechanical model and its validation with experimental $\langle 110 \rangle$ singe-crystal iron-gallium behavior, Journal of Applied Physics 103 (2008) 07–336.
[25] P. Evans, M. Dapino, Efficient model for field-induced magnetization and magnetostriction of Galfenol, Journal of Applied Physics 105 (2009) 113901.
[26] F. Ossart, R. Davidson, S. Charap, A 3D moving vector Preisach hysteresis model, IEEE Transactions on Magnetics 31 (3) (1995) 1785–1788.
[27] C. Appino, M. Valsania, V. Basso, A vector hysteresis model including domain wall motion and coherent rotation, Physica B 275 (1–3) (2000) 103–106.
[28] R. Smith, M. Dapino, T. Braun, A. Mortensen, A homogenized energy framework for ferromagnetic hysteresis, IEEE Transactions on Magnetics 42 (4) (2005) 1747–1769.
[29] R. Smith, M. Dapino, A homogenized energy model for the direct magneto-mechanical effect, IEEE Transactions on Magnetics 42 (8) (2006) 1944–1957.
[30] W.S. Oates, X. Peng, A multi-axial ferroelastic switching model using the homogenized energy approach, Proceedings of SPIE 7286 (2009), http://dx.doi.org.10.1117/12.815806.
[31] J. Atulasimha, A. Flatau, R. Kellogg, Sensing behavior of varied stoichiometry single crystal FE-Ga, Journal of Intelligent Material Systems and Structures 17 (2) (2006) 97–105, http://dx.doi.org/10.1177/1045389X06051075.
[32] J. Atulasimha, A. Flatau, Experimental actuation and sensing behavior of single-crystal iron-gallium alloys, Smart Materials and Structures 19 (2008) 1371–1381.
[33] C. Kittel, Physical theory of ferromagnetic domains, Review of Modern Physics 21 (4) (1949) 541–583, http://dx.doi.org/10.1103/RevModPhys.21.541.
[34] R. Smith, A. Hatch, B. Mukherjee, S. Liu, A homogenized energy model for hysteresis in ferroelectric materials: general density formulation, Journal of Intelligent Material Systems and Structures 16 (2005) 713–732.